Effective photoexcitation cross section of $^{115}\mathrm{In}(\gamma,\gamma')^{115\mathrm{m}}\mathrm{In}$ from photoactivation data

M. Versteegen[1,a], D. Denis-Petit[2,1], V. Méot[2], T. Bonnet[1,2], M. Comet[1,2], F. Gobet[1], F. Hannachi[1], P. Morel[2], M. Martini[3], S. Péru[2], M. Tarisien[1], and M-M. Aléonard[1]

[1] *Université de Bordeaux, CNRS-IN2P3, CENBG F-33175 Gradignan, France*
[2] *CEA, DAM, DIF F-91297 Arpajon, France*
[3] *CEA, DSM/IRFU/SPhN/ESNT, F-91191 Gif sur Yvette Cedex*

Abstract. Photoexcitation yields of the ^{115m}In metastable state were measured with Bremsstrahlung γ beams over a range of endpoint energies between 4.5 and 18 MeV. An effective cross section of the $^{115}\mathrm{In}(\gamma,\gamma')^{115m}\mathrm{In}$ photoexcitation cross section was determined to reproduce the data. This cross section is built from a cross section calculated with the TALYS code, to which an enhancement is added at about 8.5 MeV.

1 Introduction

The production of radioactive nuclei is the basic principle of nuclear activation diagnostics. The yield of activated nuclei is measured after irradiation and is used to extract the energy distribution and absolute number of particles of the incident beam, provided the cross section of the activation reaction is well known [1].

The ^{115}In is a perfect candidate for nuclear activation diagnostics. It is a stable and easy to handle isotope, with a first excited isomeric state lying 336 keV above the ground state with a half-life of 4.49 h. It is already used for the characterization of irradiation facilities [2], and as an activation standard in the context of inertial fusion experiments [3, 4]. The cross section of the $^{115}\mathrm{In}(n,n')^{115m}\mathrm{In}$ neutron inelastic scattering reaction is well known [5], and the production yield of ^{115m}In is measured to determine the yield of the 2.45 MeV fusion neutrons, emitted in DD fusion reactions. In the context of laser-matter experiments, high intensity Bremsstrahlung γ sources are also produced [6]. These sources are characterized by large numbers of particles emitted in bunches of the order of a few ps or fs, with continuous energy distributions. We investigate the possibility of using the production of the ^{115m}In isomer by photoexcitation to constrain the low energy part of the absolute energy distributions of these γ beams.

For such purposes, the $^{115}\mathrm{In}(\gamma,\gamma')^{115m}\mathrm{In}$ photoexcitation cross section has to be well known. However, surprisingly little and contradictory information is available. Early studies from the mid-1950s show a peak-shaped cross section, with a maximum of a few mb at about 8-10 MeV but disagree on the exact value of the maximum as well as on its position [7, 8]. A renewed interest in photoactivation and nuclear resonance fluorescence experiments on isomers led to several studies in the late 1980s and

[a] e-mail: versteeg@cenbg.in2p3.fr

early 1990s on ^{115}In [9–11]. Contradictory results about a second maximum in the ^{115}In$(\gamma,\gamma')^{115m}$In cross section at 22 MeV, well beyond to the Giant Dipole Resonance, are reported [12, 13], but have recently been contradicted [14].

New experimental data are needed to clarify these results. Irradiations of natural In samples were performed at the ELSA electron linac of CEA/DAM in Arpajon, France [15]. The measured photoexcited yields of ^{115m}In are compared with calculated yields obtained using different models of the cross section. As all calculated yields fail to reproduce the data, an effective cross section is built. The cross section is enhanced at low energies by means of an additionnal lorentzian contribution, the parameters of which are determined by minimizing a χ^2 between measured and calculated yields.

Section 2 describes the set up of the experiment as well as the measured data. Section 3 summarizes the data analysis, and presents the measured yields of photoexcited ^{115m}In. Section 4 shows the available photoexcitation cross sections and presents the effective cross section which allows to reproduce the data.

2 Experiment Set Up

The mono-energetic electron beam of the radio-frequency electron linac ELSA is delivered with energies up to 19 MeV with very low dispersion (0.05% RMS) using four RF cavities. In this experiment, beam intensities between 1.6 and 3.3 μA were set depending on beam energy, which varied between 4.5 and 18 MeV.

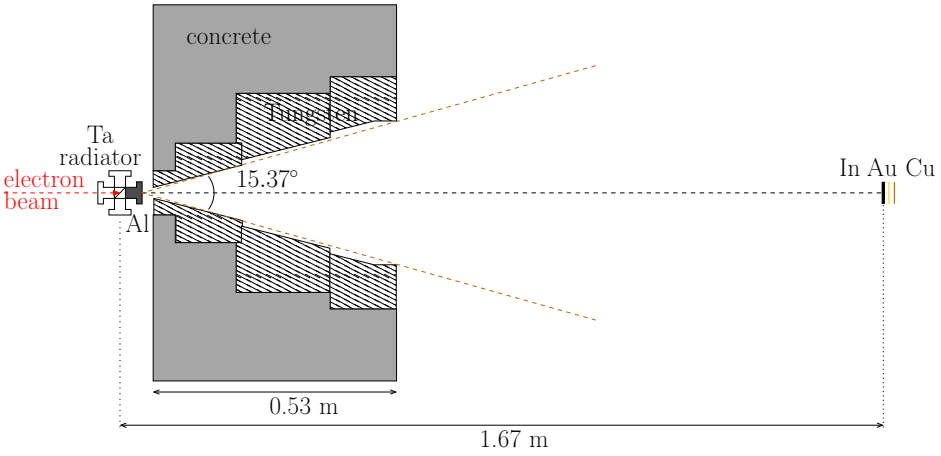

Figure 1: Set up of the experiment.

As presented on Fig.1, the electron beam is focused onto a 1.2 mm thick tantalum radiator with an angle of incidence of 45° to produce Bremsstrahlung photons. A cylindrical aluminum hardener 40 mm in length is placed against the radiator to absorb low energy photons as well as high energy electrons passing through. The photon beam is collimated by four cone-shaped collimators mainly composed of tungsten and embedded in the 0.53 m thick concrete wall separating the accelerator cave from the experimental area. The resulting opening angle of the photon beam is about 15°.

Natural indium, gold and copper samples were irradiated simultaneously at 1.67 m from the radiator, during 20 min to 2 h depending on beam energy. The gold and copper samples serve as references

for the determination of the photon flux. The targets were disk-shaped, 2.5 cm in diameter. The natural In (95.71% of ^{115}In and 4.29% of ^{113}In) targets were 3 mm thick, with typical masses of 11 g, while the ^{197}Au and natural Cu (69.15% of ^{63}Cu and 30.85% of ^{65}Cu) were 0.1 mm thick, with typical masses of 0.9, respectively 0.4 g.

Sample activation was measured offline. The γ-ray decay spectra of activated In and Au samples were each measured using high-purity coaxial, respectively broad range, HPGe detectors, with relative efficiencies of 80%, respectively 85%. Irradiated In targets were placed at a distance of 6.5 cm from the detector entrance window for counting, and the Au targets at 15.1 cm. Each detector was protected from ambient radioactivity by an 11 cm thick shielding, composed of 10 cm of Pb and 1 cm of Cu. The acquisition dead time was under 0.1% and will be neglected in the following analysis.

The β^+ activity of the Cu targets corresponding to the ^{64}Cu and ^{62}Cu daughter nuclei of the Cu(γ, n) reactions was measured using the multidetector NATALIE [1]. The two 511 keV annihilation photons are detected in coincidence by two NaI detectors, with an efficiency of 5.6±0.2% or 5.9±0.2% for ^{62}Cu or ^{64}Cu respectively. The two radioactive isotopes are identified in the time decay spectrum by their half-lives, equal to 762.06(2) min for ^{64}Cu and 9.673(8) min for ^{62}Cu.

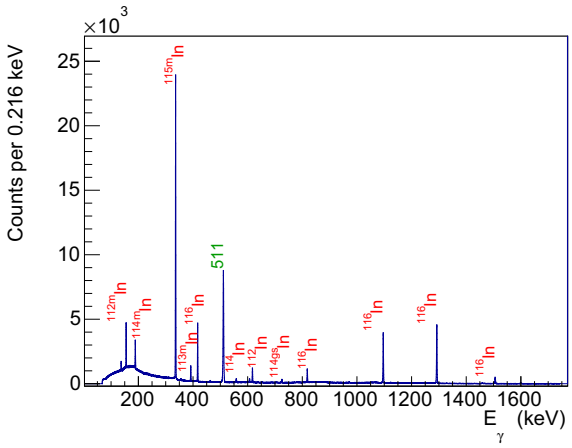

Figure 2: Decay spectrum of a natural In target irradiated at 17 MeV, measured offline during 15h of counting. The main decay lines are directly identified to the In isotope they originate from.

Figure 2 shows an example of a γ-ray decay spectrum from an In sample irradiated at the electron beam energy of 17 MeV, measured offline during 15h of counting. The photopeaks at 156, 190, 336 and 392 keV correspond to the isomeric states of ^{112m}In, ^{114m}In, ^{115m}In and ^{113m}In respectively. The ^{112}In and ^{114}In isotopes are produced by (γ, n) reactions on ^{113}In and ^{115}In present in the sample. Photopeaks at 417, 818, 1096, 1292 and 1506 keV are also observed, and correspond to the decay products of excited ^{116}In, produced by (n, γ) reactions on ^{115}In. The photopeaks at 559 and 725 keV sign the decay of ^{114gs}In, while the ones at 607 and 617 keV sign the decay of ^{112gs}In.

3 Data Analysis

3.1 Activation yields

The measured activation yield is determined from the measured number of counts in the full-energy peak corresponding to the radionuclide decay, N_γ, by:

$$Y_{act} = \frac{t_{\rm irr}}{Q} \frac{\lambda}{1 - e^{-\lambda t_{\rm irr}}} e^{\lambda t_{\rm loss}} \frac{N_\gamma - N_{bg}}{I_\gamma \epsilon (1 - e^{-\lambda t_{\rm meas}})} \quad (1)$$

if the radionuclide is populated by only one process. In Eq.(1), $t_{\rm meas}$ is the duration of counting, I_γ is the absolute γ-ray intensity, λ is the decay constant, ϵ is the detector photopeak efficiency, and Q is the total beam charge delivered during irradiation. The values of I_γ and λ are taken from Refs. [16–18] depending on the radionuclide. The background underlying the full-energy peak, N_{bg}, is taken into account, as well as decay losses during irradiation ($t_{\rm irr}$) and between the end of irradiation and the beginning of counting ($t_{\rm loss}$). The obtained yields are determined in each target sample and normalized per μC of incident electron beam.

The measured yields of ^{115m}In are compared to expected yields determined by:

$$Y_{act}(E_e) = N_{tgt} \int_{E_{\rm thres}}^{E_e} \frac{dN_\gamma}{dE_\gamma}(E_\gamma, E_e)\, \sigma(E_\gamma)\, dE_\gamma \quad (2)$$

where dN_γ/dE_γ is the Bremsstrahlung distribution of the impinging photons, with endpoint energy E_e corresponding to the electron beam energy, $\sigma(E_\gamma)$ the activation cross section at the photon energy E_γ and $E_{\rm thres}$ the reaction threshold energy. N_{tgt} is the target areal density. The calculated yield can be expressed per μC of incident electron beam when the Bremsstrahlung spectrum is normalized to the total electron beam charge.

3.2 Detector efficiencies

As shown in Eq.(1), the absolute photopeak efficiencies ϵ of the counting set-ups are necessary to determine the absolute activation yields obtained in the experiment. These efficiencies are obtained using Monte Carlo simulations to take the extended source geometry into account. The exact dimensions of the broad range and the coaxial HPGe detectors were determined using X-ray radiographies to ascertain crystal dimensions, endcap-to-crystal distances and endcap thickness. Efficiencies were calculated in the 0.12 to 1.4 MeV energy range using GEANT4 v.9.6.p03 [19]. They were compared to measured data from point-like calibration ^{152}Eu sources at four different source-to-detector distances : 15.1, 20.1, 25.1 and 30.1 cm for the broad range HPGe, and 6.5, 11.5, 16.5 and 21.5 for the coaxial HPGe.

In the case of the broad range HPGe detector, measured and calculated efficiencies were found in agreement over the whole energy range when the source-to-detector distance was beyond 20 cm. At a distance of 15.1 cm, which corresponds to the ^{196}Au activity measurement, a constant correction of about 20% had to be applied to the simulation to render measured point-like source efficiencies.

In the case of the coaxial HPGe detector, the simulated efficiencies were overestimated compared to measurements by a constant factor of 1.37 ± 0.02 over the whole energy range and at all source-to-detector distances. As the correction factor showed no dependence with energy or source-to-detector distance, it was applied to simulated efficiencies in the extended source geometry for the In samples at a distance of 6.5 cm.

Table 1. summarizes the obtained efficiencies for the decay peaks pertinent to this work. They are of the order of 1.8%, and 0.7%, for the coaxial, respectively broad range, HPGe, with uncertainties of the order of 0.02% related to statistics and to the correction factor described above.

Table 1: Absolute photopeak efficiencies in extended source geometry of the HPGe detectors used in this work.

reaction or excitation process	E_γ (keV)	ϵ (%)
^{113}In$(\gamma, n)^{112m}$In	156.61 (3)	1.82 (3)
^{115}In$(\gamma, n)^{114m}$In	190.27 (3)	1.87 (2)
^{115}In$(\gamma, \gamma')^{115m}$In	336.244(17)	1.55 (2)
^{197}Au$(\gamma, \mathrm{n})^{196}$Au	355.73 (5)	0.70 (1)

3.3 Neutron production yields

The total measured yield of ^{115m}In is the sum of the contributions from excited nuclei produced by photoexcitation and by neutron inelastic scattering reactions. These contributions are undistinguishable and the latter needs to be evaluated. To do so, all possible sources of impinging neutrons are identified.

To evaluate the excitation yields due to photo-neutrons produced by (γ, n) in the beam structures, irradiation configurations were modified. At each electron beam energy, irradiations were performed with and without shielding the targets by a 5 cm thick block of polyethylene (CH), acting as a neutron moderator, and a 1 cm thick foil of cadmium, acting as an absorber of the moderated neutrons. This shielding was placed in the beam path in front of the In sample. The expected impact on the photon spectrum at E_e = 18 MeV was determined by Monte Carlo simulations using GEANT4 and was shown to be a constant transmission of 90 ± 7% over all photon energies of the Bremsstrahlung spectrum. The uncertainty corresponds to the standard deviation. Similar simulations were performed for the expected neutron spectrum using MCNPx. The ratio between calculated neutron spectra with and without the shielding is 30 ± 10% over all neutron energies.

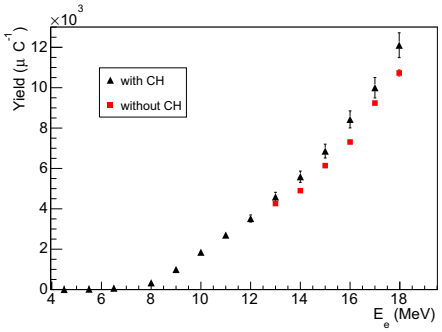

(a) Total measured excitation yields of ^{115m}In with and without the polyethylene (CH) and cadmium neutron shielding in front of the target during irradiation.

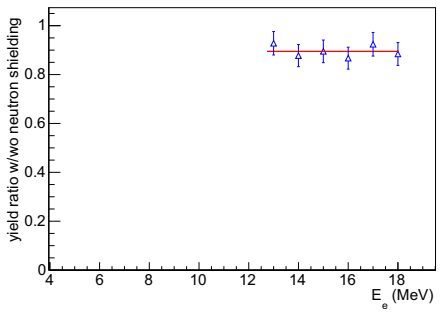

(b) Ratio between measured photoexcitation yields of ^{115m}In with and without the neutron shielding. The red line is a fit by a constant, which gives a mean ratio of 89±1%.

Figure 3

Figure 3a shows the obtained total yields of ^{115m}In with and without the neutron shielding, while Fig. 3b shows the ratio between these yields at electron beam energies above the neutron emission threshold energy. The mean ratio obtained over all electron beam energies is of the order of 90%, which is in agreement with the transmission of the photon spectra. The (n, n') cross section is of the order of 300 mb over the 2 to 10 MeV neutron energy range [20], which is about two orders of magnitude larger than the maximum value of the (γ, γ') cross sections, which is of the order of a few mb. The attenuation of the measured yields is thus not compatible with the expected attenuation of an impinging neutron spectrum, and the contribution of (n, n') excitations induced by neutrons coming from the beam structures is neglected in the following.

The yields of photoneutrons produced within the targets themselves are obtained from the measured yields of all (γ, n) reaction products. The (γ, n) reactions in the Au and Cu samples produce the ^{196}Au, ^{63}Cu and ^{65}Cu isotopes, the yields of which are already specifically measured to serve as reference for the calculation of the Bremsstrahlung spectra. The yields of ^{112m}In and ^{114m}In are determined from the measured number of counts in the 156 and 190 keV full-energy peaks in the measured decay spectrum of the irradiated In sample, using Eq.(1). The yield of ^{112gs}In is deduced from the time decay analysis of the 617 keV γ-ray line, which depends on the ^{112m}In and ^{112gs}In production yields. The production yields ^{114gs}In can not directly be extracted from measured data, as ^{114gs}In mainly de-

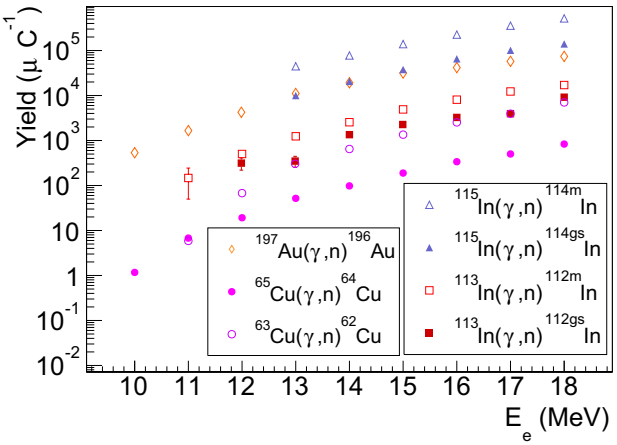

Figure 4: Production yields of photoneutrons in the In, Au and Cu samples.

cays onto the stable ^{114gs}Sn with a half life of about 71 ns [17]. An expected ratio between ^{114gs}In and ^{114m}In production yields is thus calculated using Eq.(2). The Bremsstrahlung photon fluxes are calculated, using Monte Carlo simulations, and are validated by the Au and Cu data, which are activation standards [21–23]. Cross sections of the ^{115}In$(\gamma, n)^{114gs}$In and ^{115}In$(\gamma, n)^{114m}$In reactions are calculated using the TALYS code [24], with input parameters which will be discussed in Section 4. The calculated ratio between ^{114gs}In and ^{114m}In yields is of the order of 27% over the 10 to 18 MeV energy range. This ratio is applied to the measured yields of ^{114m}In to obtain the ones of ^{114gs}In. Figure 4 presents the obtained photoneutron production yields, corresponding to the above-mentioned reactions. A total of 7×10^5 neutrons per μC of electron beam is produced in the samples in the worst case of $E_e = 18$ MeV. The (n, n') cross section and Monte Carlo simulations are used to determine the

corresponding yield of ^{115m}In produced by $(n\ n')$ excitation processes in the In sample, as described in the following.

3.4 ^{115m}In photoexcitation yields

In order to evaluate the yield of ^{115m}In produced by neutron inelastic scattering, Monte Carlo simulations using the GEANT4 code are performed. Neutrons are emitted isotropically within each sample volumes following the energy distributions of photoneutrons produced by (γ, n) reactions predicted by the TALYS code. The energy of the each neutron interacting in the In sample by neutron inelastic scattering is retrieved to build the energy distributions of interacting neutrons. These distributions

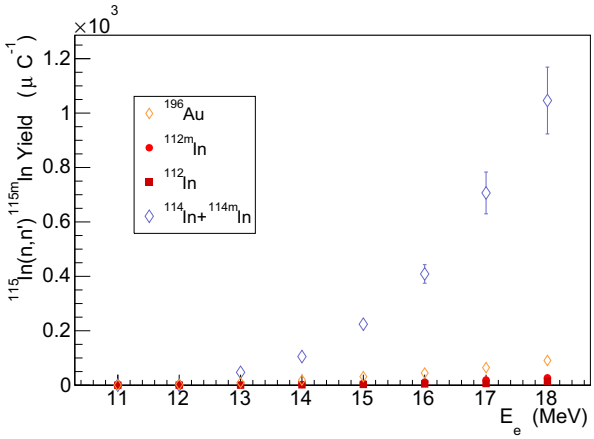

Figure 5: (Color online) Evaluated yields of ^{115m}In excited by (n, n') neutron inelastic scattering process, from photoneutrons produced in the Au and In samples.

are used to calculate the yield of ^{115m}In produced by the ^{115}In$(n, n')^{115m}$In process using an equation similar to Eq. (2), with the yields of photoneutrons presented in Fig.4 and the cross section from [20]. Details of the procedure will be published elsewhere [25]. The obtained yields are presented in Fig.5. The contribution from photoneutrons produced by the ^{115}In$(\gamma, n)^{114gs}$In and ^{115}In$(\gamma, n)^{114m}$In reactions within the In sample is the major one. The contribution from photoneutrons produced in the Au sample are one order of magnitude lower at E_e = 18 MeV.

These contributions are subtracted to the total measured yield of ^{115m}In, determined from the measured number of counts in the 336 keV full-energy peak (Eq.(1)), as presented on Fig.6. At 18 MeV, the contribution due to (n, n') reactions corresponds to about 10% of the total measured yield of ^{115m}In. This contribution decreases with decreasing electron beam energy, and is negligible below 11 MeV.

4 ^{115m}In photoexcitation cross section

The measured yields of photoexcited ^{115m}In are compared with calculated yields, obtained following Eq.(2) with the cross sections presented in Fig.7 and the calculated Bremsstrahlung spectra.

Figure 7a presents the photoexcitation cross sections from Refs. [7, 8, 26], in a figure extracted from Ref. [14]. These cross sections were obtained from activation data and show large discrepancies.

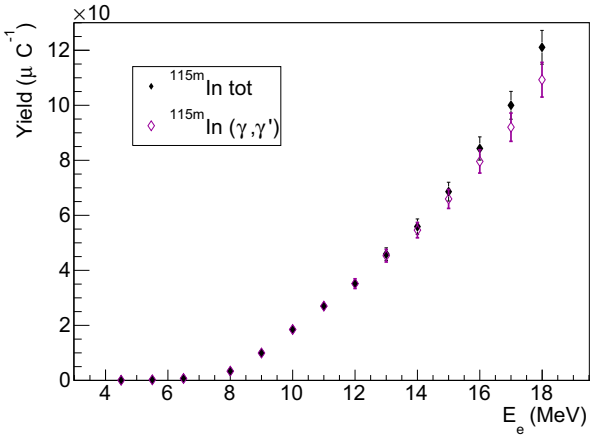

Figure 6: Total and (γ, γ') yields of ^{115m}In excited in the sample per μC of electron beam.

Authors from Ref. [8] estimate the uncertainty on σ_2 in the peak region at ~30%, and the uncertainty on the position and full width at half maximum of the peak to be ±1 MeV. The cross section σ_1 from

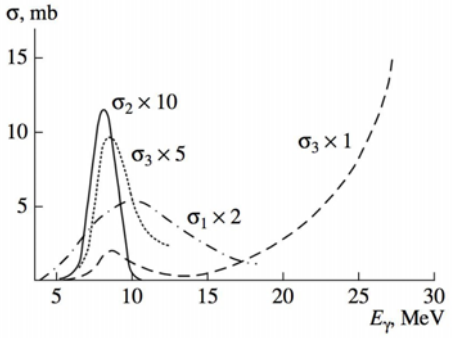

(a) Experimental cross sections, extracted from [14], with σ_1 from Ref. [7], σ_2 from Ref. [8] and σ_3 from Ref. [26].

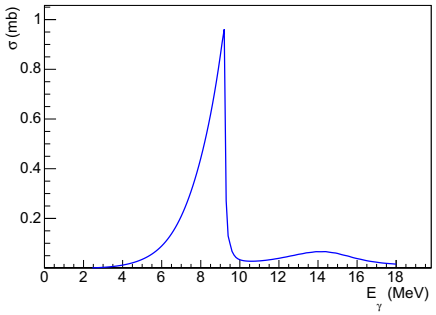

(b) Calculated cross section, obtained with the TALYS code [24], using the GLO photon strength function. See text for details.

Figure 7: ^{115}In$(\gamma, \gamma')^{115m}$In cross sections.

Ref. [7] presents a maximum value at 4.4 mb positioned at 9 MeV with a width at half maximum of 9 MeV. The authors mention that the uncertainty associated with their method of extraction of the cross section from the activation data can be up to 50% [27]. Authors from Ref. [8] discuss the data from Ref. [7] and argue that they are overestimated. The peak value should be at 2.2 mb [8] and the width of the peak should be narrower (see Ref. [8] for details). In Fig. 7a, the maximum value of σ_1 is neither 4.4 mb as published in Ref. [7], nor 2.2 mb as advised by the authors of Ref. [8], but 2.5 mb. As this could not be explained, the σ_1 cross section used in the following is the one directly extracted

from Ref. [7], with a maximum value of 4.4 mb. Finally, the cross section from Ref. [26] exhibits a second large peak above the Giant Dipole Resonance, which is located about 15.5 MeV in ^{115}In. This second peak is largely discussed in Ref. [14] and is contradicted.

Figure 7b presents a calculated photoexcitation cross section obtained with the TALYS 1.4 code. TALYS 1.4 performs the calculation with the global dispersive optical potential of Morillon and Romain [28]. The phenomenological constant temperature model of Gilbert and Cameron [29] is used for level densities, and standard options based on the RIPL database [30] are used for nuclear structure parameters. The generalized Lorentzian model (GLO) of Kopecky and Uhl [31] is used for the E1 γ strength function. This model is fully parametrized so as to reproduce (γ, n) data. All radiations other than E1 are treated under the Brink Axel hypothesis [32, 33] and the corresponding γ strength function takes the form of a standard Lorentzian function. The calculated cross section exhibits a maximum value of about 1 mb at 9.2 MeV, comparable to the experimental cross section of Ref. [8]. The sharp drop at energies beyond 9 MeV corresponds to the opening of the neutron emission decay channel.

The photoexcitation yields measured in this work are compared to calculated yields obtained with the experimental cross sections of Fig.7a and the calculated one presented on Fig.7b. These yields are presented in Fig.8. The lower energy points are presented in logarithmic scale in the inset. As there

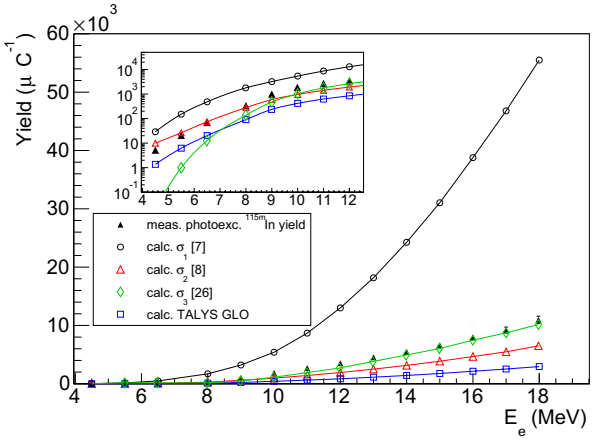

Figure 8: Comparison between photoexcitation yields of ^{115m}In measured in this work (closed black triangles) and calculated yields obtained using the (γ, γ') cross sections presented in Fig.7.

is no experimental value below 3.8 and 5.4 MeV in the σ_1 and σ_3, these cross sections supposed to drop smoothly to zero from their lowest energy point for the calculation of the yields. This hypothesis is supported by the fact that no extra photon strength is expected in the energy region below 5 MeV in ^{115}In, as none is observed in the Cd and Sn neighboring nuclei [34–36]. The yields calculated with σ_3 from Ref. [26] reproduce well our data at high energies, but fail to do so below the neutron emission threshold energy. On the contrary, the yields calculated with σ_2 from Ref. [8] reproduce the data below ~8 MeV, and are underestimated at higher energies. The cross section σ_1 from Ref. [7] was argued to be overestimated by the authors of Ref. [8], and the corresponding yields corroborate this observation, as they also are overestimated compared to the data. Even a factor of 2 on the cross

section σ_1 would not allow to reproduce the measured yields. Finally the yields obtained with the cross section from TALYS are underestimated by a factor of 4 at all electron beam energies.

In order to determine an effective photoexcitation cross section which can be used in the context of laser experiments, the calculated cross section from TALYS is modified to reproduce the data at all energies. A lorentzian function with the following expression:

$$L(E_\gamma) = \frac{1}{2\pi} \frac{A\,\Gamma}{(E_\gamma - E_0)^2 + \Gamma^2/4} \tag{3}$$

is introduced and directly added to the TALYS cross section. The parameters A, Γ and E_0 represent the normalization constant, the width and mean energy of the lorentzian function. They are adjusted to minimize a χ^2 between calculated and measured yields. Figure 9 shows the measured and calculated yields for which the minimum χ^2 value is obtained ($\chi^2/NDF = 1.2$), with the lower energy points in logarithmic scale in the inset. The calculated yields obtained using the modified cross section are in open pink circles. Measured and calculated photoexcitation yields are in very good agreement both at

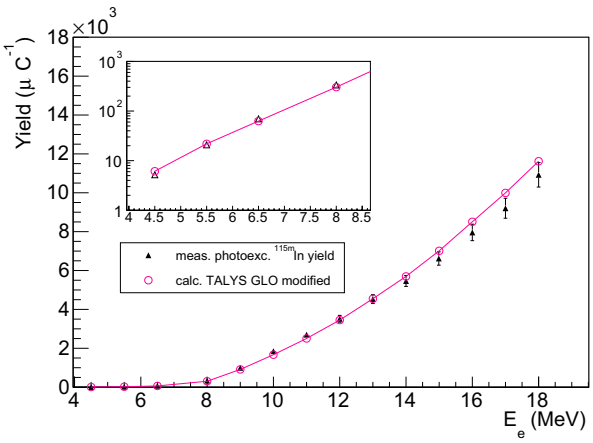

Figure 9: (Color online) Measured photoexcitation yields of ^{115m}In and calculated yields obtained with the modified cross section from TALYS. See text for details.

low and high electron beam energies. The parameters of the added lorentzian function are :

$$A = 4.3 \text{ mb} \qquad \Gamma = 0.9 \text{ MeV} \qquad \text{and} \qquad E_0 = 8 \text{ MeV}$$

Figure 10 shows the corresponding effective cross section (pink dashed line). The added lorentzian function increases the maximum of the cross section from ~1 mb at ~9.5 MeV to ~4 mb at about 8.5 MeV, compared to the cross section calculated with TALYS alone. The experimental cross sections already presented on Fig. 7a are also reported, with the extrapolation to zero introduced in this work. The σ_3 cross section from Ref. [26] which reproduced the photoexcitation yields at energies above the neutron emission threshold is comparable to the effective cross section, but falls more rapidly to zero below 5 MeV, thus explaining the underestimation of the yields at low energies. The σ_2 cross section from Ref. [8] is very similar to the effective cross section at low energies, but is lower by about a factor of four at the maximum, which is enough to underestimate the yields at high energies. The σ_1 cross section from Ref. [7] is largely overestimated, as already noted.

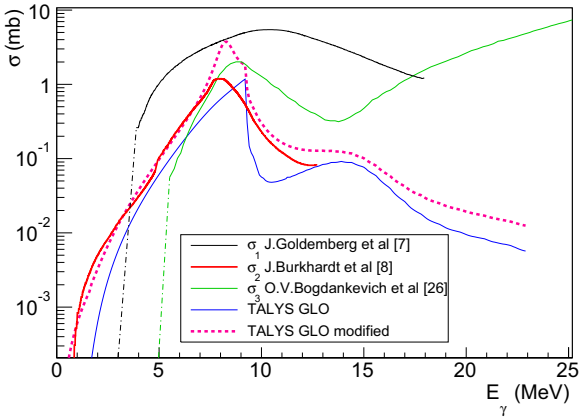

Figure 10: Cross sections of ^{115}In$(\gamma,\gamma')^{115m}$In. Extrapolations of experimental cross sections σ_1 and σ_3 in dash-dotted line were performed in this work. See text for details.

5 Conclusion

Photoexcitation yields of ^{115m}In have been measured on an energy range between 4.5 and 18 MeV using a Bremsstrahlung photon source. These yields are used to test the experimental cross sections of the (γ,γ') excitation process available in the literature, as well as a cross section obtained by calculation using the TALYS code. As none of these cross sections allows to reproduce the data on the whole energy range, an effective cross section is built by adding a lorentzian contribution to the calculated one. The parameters of this lorentzian are determined from the minimization of a χ^2 between measured and calculated yields.

The effective cross section allows to reproduce the data, but no fundamental physics motivation supports the direct modification of the cross section. However, it has been shown that additionnal strength is missing in the GLO model in neighboring nuclei, at energies around the neutron emission threshold [34–36]. Rather than directly modifying the cross section, a systematic study on the γ strength function should be performed. Such a study was carried out and will be published elsewhere [25].

References

[1] M. Tarisien, C. Plaisir, F. Gobet, F. Hannachi, M.M. Aléeonard, A. Rebii, Rev.Sci.Instrum. **82** (2011)
[2] U. Kneissl, Prog. Part. Nucl. Phys. **46**, 79 (2001)
[3] C. Ruiz et al., Rev.Sci.Instrum. **63** (1992)
[4] O. Landoas et al., Rev.Sci.Instrum. **82** (2011)
[5] N. Otuka et al., Nuclear Data Sheets **120**, 272 (2014)
[6] C. Courtois, A. Compant La Fontaine, O. Landoas, G. Lidove, V. Méot, P. Morel, R. Nuter, E. Lefebvre, A. Boscheron, J. Grenier et al., Phys. Plasmas **16**, 013105 (2009)
[7] J. Goldemberg, L. Katz, Phys. Rev. **90**, 308 (1953)

[8] J. Burkhardt, E.J. Winhold, T.H. Dupree, Phys. Rev. **100**, 199 (1955)
[9] J.J. Carroll et al., Phys. Rev. C **43**, 1238 (1991)
[10] P. von Neumann-Cosel et al., Phys. Lett. B **266**, 9 (1991)
[11] P. von Neumann-Cosel, V.Y. Ponomarev, A. Richter, C. Spieler, Z. Phys. A **350**, 303 (1995)
[12] L. Lakosi, J. Sáfár, A. Veres, T. Sekine, H. Kaji, K. Yoshihara, J. Phys. G: Nucl. Part. Phys. **19**, 1037 (1993)
[13] V. Bokhinyuk, A. Guthy, A. Parlag, M. Sabolchy, I. Sokolyuk, I. Khimich, Ukr. J. Phys. **51**, 657 (2006)
[14] L.Z. Dzhilavyan, Phys. Atom. Nucl. **78**, 624 (2015)
[15] A. Chauchat, V.L. Flanchec, A. Binet, J. Flament, P. Balleyguier, J. Brasile, S. Muller, J. Ortega, Nucl. Instrum. Meth. A **608**, S99 (2009)
[16] S. Lalkovski, F. Kondev, Nuclear Data Sheets **124**, 157 (2015)
[17] J. Blachot, Nuclear Data Sheets **113**, 515 (2012)
[18] J. Blachot, Nuclear Data Sheets **113**, 2391 (2012)
[19] S. Agostinelli et al. (GEANT4), Nucl. Instrum. Meth. **A506**, 250 (2003)
[20] M. Bhike, A. Saxena, B.J. Roy, R.K. Choudhury, S. Kailas, S. Ganesan, Nucl. Sci. Eng. **163**, 175 (2009)
[21] C. Nair, M. Erhard, A.R. Junghans, D. Bemmerer, R. Beyer, E. Grosse, J. Klug, K. Kosev, G. Rusev, K.D. Schilling et al., Phys. Rev. C **78**, 055802 (2008)
[22] R.E. Sund, M.P. Baker, L.A. Kull, R.B. Walton, Phys. Rev. **176**, 1366 (1968)
[23] C. Plaisir, F. Hannachi, F. Gobet, M. Tarisien, M. Aléonard, V. Méot, G. Gosselin, P. Morel, B. Morillon, Eur. Phys. J. A **48**, 68 (2012)
[24] S.H. A.J. Koning, M. Duijvestijn, *TALYS-1.0*, in *Proceedings of the International Conference on Nuclear Data for Science and Technology April 22-27, 2007, Nice, France* (editors O.Bersillon, F.Gunsing, E.Bauge, R.Jacqmin, and S.Leray, EDP Sciences, 2008), pp. 211–214
[25] M. Versteegen et al., to be published
[26] O.V. Bogdankevich, L.E. Lazareva, F. Nikolaev, Sov. Phys. JETP **4**, 320 (1956)
[27] H.E. Johns, L. Katz, R.A. Douglas, R.N.H. Haslam, Phys. Rev. **80**, 1062 (1950)
[28] B. Morillon, P. Romain, Phys. Rev. C **70**, 014601 (2004)
[29] A. Gilbert, A.G.W. Cameron, Can. J. Phys. **43**, 1446 (1965)
[30] R. Capote et al., Nuclear Data Sheets **110**, 3107 (2009)
[31] J. Kopecky, M. Uhl, Phys. Rev. C **41**, 1941 (1990)
[32] D. Brink, Nucl. Phys. **4** (1957)
[33] P. Axel, Phys. Rev. **126** (1962)
[34] A.C. Larsen, I.E. Ruud, A. Bürger, S. Goriely, M. Guttormsen, A. Görgen, T.W. Hagen, S. Harissopulos, H.T. Nyhus, T. Renstrøm et al., Phys. Rev. C **87**, 014319 (2013)
[35] H.K. Toft, A.C. Larsen, A. Bürger, M. Guttormsen, A. Görgen, H.T. Nyhus, T. Renstrøm, S. Siem, G.M. Tveten, A. Voinov, Phys. Rev. C **83** (2011)
[36] H.K. Toft, A.C. Larsen, U. Agvaanluvsan, A. Bürger, M. Guttormsen, G.E. Mitchell, H.T. Nyhus, A. Schiller, S. Siem, N.U.H. Syed et al., Phys. Rev. C **81**, 064311 (2010)